Improvement of gas barrier properties of chitosan-based composite coatings under humid conditions through palmitic acid grafting

Fatima Essabti, Alain Guinault, Sébastien Roland, Matthieu Gervais

European Polymer Journal xxx (xxxx) 113769

Contents lists available at ScienceDirect

European Polymer Journal

journal homepage: www.elsevier.com/locate/europolj

Improvement of gas barrier properties of chitosan-based composite coatings under humid conditions through palmitic acid grafting

Fatima Essabti, Alain Guinault, Sébastien Roland, Matthieu Gervais *

Laboratory PIMM, CNRS, Arts et Métiers Institute of Technology, Cnam, 75013 Paris, France

ARTICLE INFO

Keywords:
Chitosan
Palmitic acid
Grafting
Vermiculite
Barrier properties
Coating

ABSTRACT

The chemical grafting of palmitic acid (PA) on chitosan (CS) was performed through the coupling reaction of the carboxyl group of PA with the amine groups of CS in the presence of 1-ethyl-3-(3-dimethylaminopropyl) carbodiimide (EDC). Fourier Transform InfraRed (FTIR), Differential Scanning Calorimetry (DSC) and ^{13}C NMR spectroscopies were used to analyze the synthesized chitosan-grafted-palmitic acid (CS-g-PA). Acidified aqueous solutions of CS, a mix of CS and PA (CS/PA) and CS-g-PA (1 wt%), in the presence of different contents of vermiculite (VMT), have been coated on 130 μm thick corona-treated PET films with thicknesses ranging from 1 to 3 μm. Gas permeability of the PET coated films were determined under dry conditions and under different relative humidity ratios. The grafted CS exhibited a higher hydrophobicity which resulted in a fewer loss of barrier properties in humid conditions.

1. Introduction

Gas permeability of plastics is a property highly studied currently due to its implication in many applications such as food, cosmetic packaging, hydrogen storage or helium-based weather balloons. Specific high gas barrier polymers, such as poly(vinyl alcohol) (PVOH) and its copolymers with ethylene (EVOH) or coatings based on poly(vinylidene chloride) (PVDC), are usually employed [1]. However, the need for innovative solutions is still present as those petroleum-based solutions show limitations either due to moisture sensitivity, brittleness or potential toxicity.

New bio-based polymers and their associated composites with mineral particles, such as montmorillonites are developed to answer some of those issues. In particular, chitosan-based materials have encountered a great interest in the literature in the recent years [2,3]. Chitosan (CS) is indeed currently largely studied for its use in many applications such as food, pharmaceutical, cosmetics or agriculture. Its important availability, renewability and biocompatibility have made this polymer one of the most studied polysaccharides. The presence of hydroxyl functions on its backbone also leads to high gas barrier properties that have made this material a good candidate to create more environmentally friendly food packaging [4]. However, the main drawback of its structure is a high dependency to relative humidity with a quick loss of its properties due to a plasticizing effect of moisture.

To overcome this issue, chemical modification of these hydroxyl functions has been envisaged to decrease the hydrophilicity of the polymer. Indeed, the presence of reactive functional groups combined with the polysaccharide nature of CS leads to numerous chemical modifications. Amine groups can cause chemical reactions such as alkylation, quaternization, reaction with aldehydes and ketones, grafting, etc. Moreover, the hydroxyl moieties can also lead to some reactions such as acetylation, crosslinking, grafting, etc. [5–7]. Grafting is one of the most studied and promising approaches for a wide variety of molecular models [7–10] and seems to be an important technique to modify the chemical and physical properties of CS, widening its use in many applications. Although, the functional properties, including antioxidant and antimicrobial activities of grafted CS, have been well studied, practical applications of grafted CS in various areas especially for its barrier properties are rarely reported. Only crosslinking with poly(acrylic acid) has been reported to overcome the moisture sensitivity of CS [11]. To date, several types of acids including gallic acid [12–17], caffeic acid [12,16,18–20], ferulic acid [16,21–24], catechin acid [20,25], salicylic acid [26,27], eugenol acid [28,29], phloroglucinol acid [30], coumaric acid [31] and tannic acid [32] have been successfully grafted to CS. The chemical modification by copolymerization of CS is of great interest as it allows expanding its application field.

In this study, palmitic acid (PA) was grafted onto chitosan (CS) to maintain the gas barrier properties of CS under humid conditions. PA is a stable saturated fatty acid with a 16-carbon chain and is easier to ma-

* Corresponding author.
E-mail address: matthieu.gervais@lecnam.net (M. Gervais).

https://doi.org/10.1016/j.eurpolymj.2025.113769

Received 16 September 2024; Received in revised form 23 December 2024; Accepted 23 January 2025
0014-3057/

nipulate than unsaturated fatty acids due to its resistance to oxidation. The grafting reaction was initiated using N-(3-dimethylaminopropyl)-N'-ethylcarbodiimide (EDC), which activates carboxylic acid groups to form amide bonds with primary amines on CS [33]. To further improve the barrier properties of CS coatings, nanofillers such as clays have been explored [34]. In previous work, the addition of up to 50 wt% vermiculite (VMT) significantly enhanced the oxygen barrier properties of CS coatings in dry conditions [35]. This study investigates the combination of CS and CS-g-PA coatings on PET films, followed by the incorporation of nanocomposites based on CS/VMT and CS-g-PA/VMT. The effects of varying filler content (up to 60 wt%) on the helium and oxygen gas barrier properties were evaluated, with a particular focus on helium permeability under humid conditions, as this is of real interest for applications such as weather balloons containing helium, which require high gas barrier performance despite varying humidity.

2. Materials and methods

2.1. Materials and reagent

VMT water dispersion (MicroLite 963 – dry content 9 wt%) used in this work was supplied by Specialty Vermiculite Corp Company, Canada. Granulometry varies in the range of 0.5–15 mm and % OSP (Over Sized Particles refers to the percentage of particles retained on a 45-μm screen) was ≤ 8 %. CS was obtained from the shrimp shell by Glentham Life Sciences (Wiltshire, United Kingdom), ($\overline{M_w}$ = 890 000 kDa; viscosity: 0.1–0.3 Pa.s and degree of deacetylation > 95 %). Acetic acid (glacial 100 %, Merck, Darmstadt, Germany), N-(3-dimethylaminopropyl)-N'-ethylcarbodiimide (EDC) (≥97.0 %, Sigma-Aldrich, USA), ethanol (MM: 46,07 g/mole, Sigma life Science) and palmitic acid (99+ %, Sigma-Aldrich, USA) were used as received. A commercial 130 μm poly(ethylene terephthalate) (PET) film was coated respectively with CS, CS-g-PA solutions and CS/VMT, CS-g-PA/VMT solutions. No further purification of chemicals has been realized and freshly prepared solutions were always used.

2.2. Grafting of palmitic acid on CS

The grafting of palmitic acid on amine functions of CS has been carried out following the procedure described in the literature [33]. Typically, 1 g of CS powder was dissolved in 50 mL of an acetic acid aqueous solution 1 %(v/v). 0.3 g of palmitic acid (1.17. 10^{-3} mol) was dissolved in 30 mL of ethanol which corresponds to 19 mol% compared to amine groups (6.2. 10^{-3} mol) carried by CS units as calculated by Equation (1), considering $M_{Chitosan\ unit}$ = 161 g/mol and $M_{Palmitic\ acid}$ = 256 g/mol.

$$\frac{Palmiticacid}{chitosan} mol\% = \frac{\frac{m_{Palmiticacid}}{M_{Palmiticacid}}}{\frac{m_{chitosan}}{M_{chitosanunit}}} \quad (1)$$

The two solutions were mixed at 80 °C under magnetic stirring prior to the addition of 0.25 g of EDC ($1.6.10^{-3}$ mol) and the reaction was then conducted for 6 h. The solution was then dialyzed using dialysis membrane (Spectra/Por® 6 (MWCO 1– 50KD), Spectrum Laboratories, USA) against distilled ethanol first and then against water with successive exchange of fresh solvent in order to remove unreacted PA and EDC.

The CS/PA solution was prepared using similar quantities of CS and PA, i.e. 1 g and 0.3 g respectively, and solubilized in acetic acid solution 1 %(v/v) without further treatment.

2.3. Preparation of CS and nanocomposite solutions

CS solutions were prepared by dissolving 1 g of CS in 50 mL of 1 % (v/v) aqueous acetic acid solution and stirred continuously overnight at room temperature to obtain a homogenous mixture. For nanocomposites solutions, VMT particles dispersed in water (9 wt%) were diluted in the same solvent as CS. The volume of water dispersion and aqueous acetic acid dilution varies with the expected final composition of VMT (details presented in Table 1).

The resulting slurry was kept stirring for 24 h at room temperature. Finally, CS/VMT nanocomposites solutions were prepared by gradually adding diluted VMT into the CS solution at room temperature, and then the resulting mixture was stirred for another 24 h using magnetic stirrer.

2.4. Preparation of CS-g-PA and nanocomposites solutions

A quantity of 1 g CS-g-PA powder was dispersed in 50 mL of a mixture of aqueous acetic acid solutions of 1 % (v/v) and acetone (2:1 (v/v)). The solution was heated for 30 min at 50 °C, and then the solution was stirred overnight at room temperature, under continuous agitation of 1200 rpm using a magnetic stirrer. CS-g-PA/VMT nanocomposites have been prepared as previously mentioned CS/VMT nanocomposites. The prepared nanocomposites have a final VMT content of 25 and 60 wt%, as shown in Table 2.

2.5. CS/nanocomposite coated PET films

The layered films were prepared by a bar-coating technique: aqueous acetic acid 1 wt% solutions of CS or CS-VMT nanocomposites were coated with a 50 μm barcoater on 130 μm corona-treated PET films similarly to our previous work where this procedure is exhaustively described [35]. Coatings were applied by depositing two layers on top of each other with a drying step at 45 °C for 15 min under vacuum after in between the depositions. The final coating was then dried under the same conditions for 12 h.

2.6. Density measurement

Density measurements (ρ) were carried out at 23 °C. The density of the samples was determined using a density kit (Mettler-Toledo) according to Equation (2):

Table 1
Compositions and dry extracts of the various coatings.

V_{CS} initial (mL) ([CS] = 20 g/L)	$V_{initial}$ (VMT solution) (dry content 9 wt%) (mL)	$V_{(H2O/Ac\ acid\ 1\%(v/v))}$ added to VMT (mL)	[VMT] obtained (g/mL)	CS/VMT solution dry extract (g/mL)	Final VMT wt%
50	4.5	9.9	0.33	1.26	25 %
50	8.0	19.8	0.60	1.20	40 %
50	12.0	30.0	1.00	1.16	50 %
50	20.11	45.0	1.50	1.14	60 %

Table 2
Compositions and dry extracts of the various coatings of CS-g-PA/VMT.

$V_{initial\ of\ CS\text{-}g\text{-}PA}$ (mL) ([CS] = 20 g/L)	$V_{initial}$ (VMT solution) (dry content 9 wt%) (mL)	$V_{(H2O/Ac\ acid\ 1\%(v/v)/acétone\ (2:1\ (v/v))}$ added to VMT (mL)	[VMT] obtained (g/mL)	CS-PA/VMT solution dry extract (g/mL)	Final VMT (wt%)
50	4.5	9.9	0.33	1.26	25
50	20.11	45.0	1.50	1.14	60

$$\rho = m_{Sair} / \left(m_{Sair} - m_{Swater}\right) \quad (2)$$

where: m_{Sair} = apparent mass of specimen in air,
m_{Swater} = apparent mass of totally immersed specimen in water.

2.7. Differential Scanning Calorimetry measurements (DSC)

DSC measurements were carried out using a DSC Q10 (TA Instruments). The scans were performed under nitrogen atmosphere (50 mL/min) from −30 to 190 °C at a heating rate of 10 °C/min with sample mass ranging from 4 to 8 mg placed in standard aluminum pans. Before measurements, the CS, CS-g-PA and CS/PA samples were conditioned at 0 %RH at 23 °C.

2.8. Nuclear magnetic resonance (NMR)

Solid state ^{13}C NMR spectra were recorded with a Bruker Avance III spectrometer, a 7.05 T magnet and a ^{1}H-X dual-resonance MAS probe (diameter: 4 mm). The sample rotation frequency was fixed to 4 kHz. A ^{13}C direct polarization experiment was used with 5 and 10 s of repetition times. The 90° pulse (^{13}C) was 4.3 ms and the intensity of the ^{1}H dipolar decoupling applied during the acquisition of the ^{13}C NMR signal, set at 32 kHz. Chemical displacements of ^{13}C have been calibrated against TMS using an external reference, glycine: for phase a, the peak associated with carbon CO has a chemical displacement ^{13}C of 176.03 ppm. The temperature of the samples was maintained at 27 °C during the experiments.

2.9. Scanning Electron Microscopy (SEM): Observation and thickness analysis

In order to evaluate the coating thickness (PET/1 layer, PET/2 layers, and PET/3 layers), coated films were prepared using an ultramicrotome (LKB BROMMA 2088 – ULTROTOME V), equipped with a diamond knife at room temperature. Then, the film thickness of each layer was estimated using SEM (Hitachi 4800 SEM). The thicknesses were observed using an accelerating voltage of 0.7 kV and images were taken at a magnification ranging from 800 to 2000. The thicknesses reported are the average value of at least 8 measurements performed at different points of the film and at least two films for each condition has been characterized.

2.10. Helium and oxygen permeability

The helium permeability and transmission rate were measured at 23 °C and at different levels of relative humidity (RH) of 0 %, 50 %, 75 % and 98 %, by a specific home-made analyzer, based on the ISO 15105–2:2003 method. Circular portions cut from the films (surface = 23.75 cm^2) were inserted between two hermetically sealed compartments drained using nitrogen. A helium constant flow, of 80 $mL.min^{-1}$, was introduced in the downstream part of the cell and was measured in the upstream part, using a helium detector (mass spectrometer ADIXEN 142). The different relative humidity levels were fixed in the upstream part of the cell by bubbling the helium through various solutions. The solutions used for each humidity content are magnesium nitrate ($Mg(NO_3)_2$) (50 % RH), sodium chloride (NaCl) (75 % RH) and distilled water (98 % RH). A humidity control of the gas is carried out at the cell outlet by a dew-point meter (EdgeTech-DewMaster-Dew Point Chilled Mirror Hygrometer). Before carrying out the tests, the films were conditioned in desiccators containing the same solutions at the humidity levels studied up to the stability of the weight except for 98 % RH where the films were immersed directly in distilled water. The OTR (Oxygen Transmission Rate) was measured with a Systech analyzer 8001 at 23 °C and 0 % RH on film samples. Oxygen permeability was obtained by multiplying respectively the OTR by the pressure (1 bar) and the thickness.

Then, the permeability of the coated layer was calculated using Equation (3).

$$\frac{1}{P_{PETC}} = \frac{th_{PET}}{th_{PETC}} \frac{1}{P_{PET}} + \frac{th_{CL}}{th_{composite}} \frac{1}{P_{CL}} \quad (3)$$

where P_{PETC} is the permeability of coated PET, th_{PETC} the thickness of coated PET, P_{CL} the permeability of coated layer, th_{CL} the thickness of coated layer and P_{PET} the permeability of PET film and th_{PET} the thickness of PET film.

The tests were repeated three times for oxygen permeability and five times for helium permeability, with the film being replaced after each test.

3. Results and discussion

3.1. Grafting of palmitic acid on CS

The grafting reaction of palmitic acid on CS was carried out following a previously described procedure [33], as illustrated in Fig. 1. A ratio of around 20 mol% of grafting on the amine functions of CS was aimed in order to keep a majority of amine functions to maintain a solid hydrogen-bonded network in the amorphous phase of the CS to avoid the gas permeability. In order to characterize the efficiency of the grafting reaction, different analyses have been conducted on the obtained material.

To verify the efficiency of the grafting reaction, the material was analyzed using different techniques. First, FTIR analysis (Fig. 2) was conducted on CS, CS-g-PA and a blend of PA and CS. The signals associated with palmitic acid can be observed in the range of 1600–1300 cm^{-1} with especially three peaks at 1558, 1375, and 1311 cm^{-1}. Those peaks are observed for CS-g-PA and PA/CS blend as expected even after the dialysis step for CS-g-PA, where unreacted PA has been removed from the solution. A peak associated with the amide functions is observed at 1651 cm^{-1}. This peak is observed with all samples as amide functions are present in CS due to an uncomplete deacetylation of the initial chitin. However, this peak is more intense for the CS-g-PA which means that the grafting of PA with creation of amide functions occurred. In or-

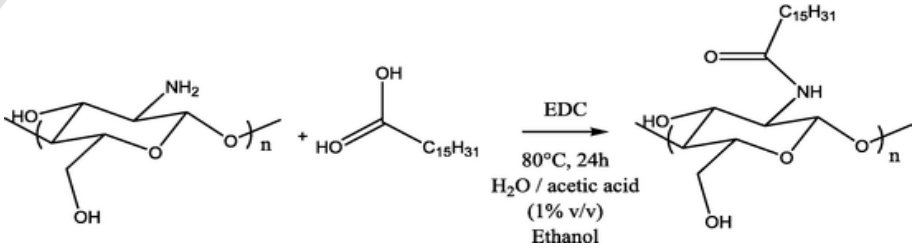

Fig. 1. Synthesis of CS-g-PA copolymer by grafting palmitic acid on CS using EDC catalyzer.

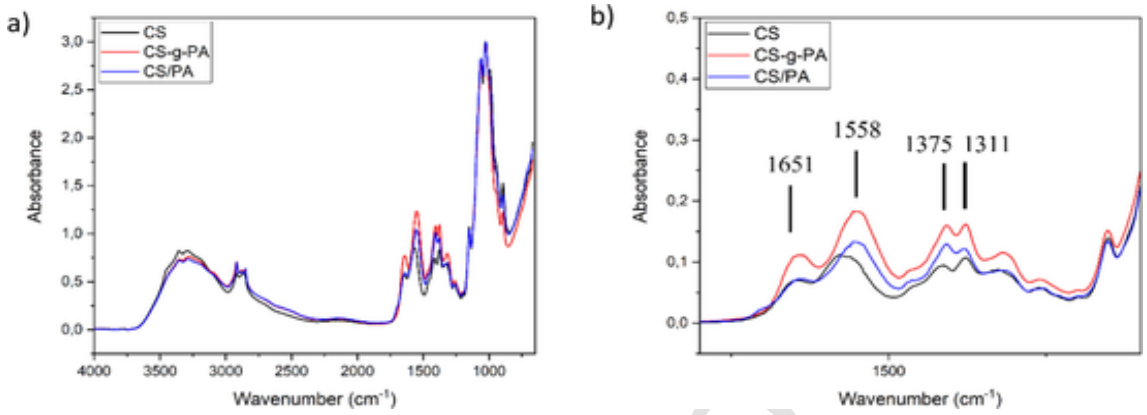

Fig. 2. Infrared spectra of CS, CS-g-PA, and CS/PA mixture: a) spectrum from 4000 to 650 cm^{-1} ; b) zoom on 1800 to 1100 cm^{-1}.

der to confirm the presence of PA in CS-g-PA after the washing steps, a solid-state NMR analysis was performed.

As the hydrophilic/hydrophobic balance of CS is expected to evolve with palmitic acid grafting, the solubility of CS-g-PA is not expected to be similar. Table 3 contains the various solvents used to solubilize CS after grafting. CS-g-PA presents a different solubility than pristine CS. CS is soluble in an acidified aqueous solution contrary to CS-g-PA which indicates an increase of hydrophobicity of this latter. This difference in solubility confirms that a chemical modification on the CS chain occurred. According to this solubility test, the solvent chosen for the solubilization of CS-g-PA is a mixture of aqueous solution of acetic acid 1 % and acetone (2: 1 (v/v)), which is used to prepare the pure films of CS-g-PA and CS-g-PA/VMT.

Due to the complex dissolution of the CS-g-PA, solid-state ^{13}C NMR analysis was carried out to study the chemical structure of the product. The spectrum of CS-g-PA is presented in Fig. 3. It corresponds to a ^{13}C direct polarization experiment with dipolar decoupling of protons and rotation at the magic angle. CS carbon contributions are presented in black. The peaks at 13.6 and 178 ppm are attributed to methyl and carbonyl carbons, respectively. Carbon C_2, linked to the N-acetyl group, gives a chemical shift of 57 ppm. The C_6, corresponding to the hydroxymethyl group, resonates at 60 ppm. Chemical shifts quite close to 74 and 74.4 ppm are attributed to C_3 and C_5 pyranose carbons, respectively. A hydroxy methyl is linked to C_5 while a hydroxyl is attached to C_3. The carbons involved in the glycosidic bond, C_4 and C_1, show chemical shifts at 83.3 and 104.3 ppm, respectively. All the peaks corresponding to CS are well found. The red peaks correspond to the different methyl groups of palmitic acid (CH_2) indicating the presence of this part on the CS-g-PA. Unfortunately, no shift of the peak corresponding to the amine function that becomes an amide function could be observed. However, since the CS was washed after the grafting reaction effectively eliminating any residual presence of unreacted palmitic acid, the presence of palmitic acid carbons (after grafting) on solid-state ^{13}C RMN spectra tends to show that the reaction did occur.

Thermal analysis was carried out by DSC to confirm the grafting reaction of palmitic acid onto the CS chain. The DSC thermograms obtained at the second heating ramp for CS, PA, and CS-g-PA are presented in Fig. 4. The thermogram of palmitic acid shows a melting peak at 65 °C. In the case of CS-g-PA, the presence of palmitic acid was confirmed by ^{13}C NMR analysis, but in the DSC analysis, no melting peak could be observed at 65 °C. On the other hand, this peak is present in

Table 3
CS-g-PA solubility tests.

Solvent	CS	CS-g-PA
H_2O	Insoluble	Insoluble
H_2O/Acetic acid (1 %)	Highly soluble	Insoluble
(H_2O/Acetic acid (1 %)/ Acetone	–	Soluble

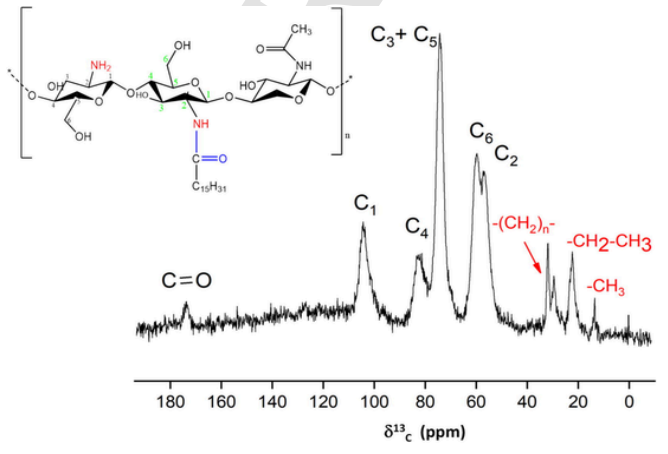

Fig. 3. ^{13}C NMR spectrum obtained in solid phase of the CS-g-PA (rotation speed of rotor 4 kHz, T = 27 °C).

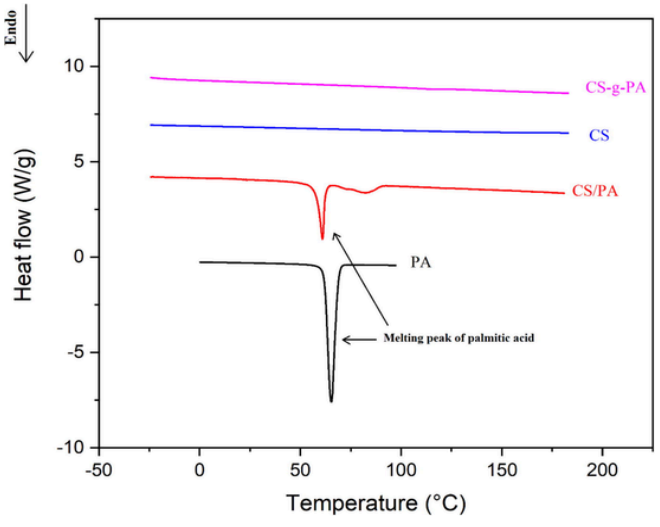

Fig. 4. DSC thermograms obtained at second scan for PA, CS-g-PA, and CS/PA mixture.

the case of the mixture between CS and PA (CS/PA) with a slight shift to lower temperature. The disappearance of the melting peak of PA in the grafted CS could be explained by the fact that its crystallization is prevented by its linkage to the CS backbone. This change in crystallization behavior tends to confirm that residual palmitic acid is well grafted on CS chains.

3.2. Structure and properties of PET coated CS-g-PA films

CS-g-PA and CS-g-PA/VMT coatings were prepared in a similar manner to non-grafted CS coatings to observe the effect of grafting on coating properties. Two VMT contents were chosen: 25 and 60 wt%. The 25 wt% will achieve a reasonable value, particularly in terms of mechanical properties and is a good compromise between barrier properties and general aspect of the coating. Previous work [35] has shown that high VMT contents (>50 wt%) significantly impact gas barrier properties. The effect of a high incorporation of hydrophilic fillers in humid conditions remains at stake here. Fig. 5 shows the images of PET films coated with two layers of CS, CS-g-PA, and CS-g-PA/VMT with different contents of VMT. It is noteworthy that PET film coated with CS-g-PA has a slightly translucent surface compared to PET film coated with CS at similar thicknesses (around 2 to 3 μm). In addition, yellow tint increases with increasing VMT content as previously observed for the non-grafted [35]. Overall, all films are visually transparent. These results are consistent with the results of CS/VMT coated PET films.

PET films were coated by two successive layers of CS-g-PA/VMT with a content of 25 and 60 wt% in VMT. The thicknesses of these layers were measured in the same way as CS/VMT coated PET films by SEM observation [35] (Fig. 6). As observed after cutting in the cross section, coated layers have a good adhesion to PET film and present no defects. In addition, these images show the absence of pores or other inclusions. It can be concluded that the quality of the grafted CS layers obtained is similar to that obtained with the non-grafted CS. However, Table 4 shows that CS-g-PA coated layers are thicker than non-grafted CS layers for the same nano-fillers content. The thickness of the CS-g-PA layer is ca. 2.5 μm. However, the thickness of the CS layer is ca. 2.1 μm, reflecting an increase of 0.4 μm with the grafted layers. After the addition of VMT, layer thickness increases to 3.01 and 2.8 μm for 25 and 60 wt% VMT, respectively. This may be due to the bar coater method (layers have been manually spread) but also to the difference in density between pure CS (1.411 g/cm^3) with very high cohesion via hydrogen bonds and CS-g-PA (1.317 g/cm^3) where grafted chains create addition spacing between molecules.

Since the coated layers with grafted CS have the same qualities as the pure CS and the thickness is also comparable, the permeability studies can be conducted in a similar manner to the previous study [35]. First, it is important to know the modification of barrier behavior indry state. Indeed, the addition of grafts on the amine functions of CS may reduce the amount of hydrogen bonds present in the material and these are responsible for the barrier properties. Fig. 7 (a) shows a comparison between the results of the oxygen transmission rate (OTR) of the PET film coated with two layers of CS, CS/VMT, CS-g-PA and CS-g-PA/VMT in dry state (23 °C and 0 % RH). According to this figure, the OTR of the grafted and non-grafted CS is perfectly superimposed, regardless of the content of nanofillers added. In addition, a PET film coated with 60 wt% VMT, where the thickness of the coated layer is of the order of 2.8 μm, exposes an OTR below the commercial instrumentation detection limit (0.008 cm^3/m^2.day). It can be concluded that these results are similar to those obtained with non-grafted CS and the properties are not degraded by the presence of grafting even if the thicknesses deposited with the grafted CS are slightly higher than those of non-grafted CS. The OTR results allow us to calculate the permeability of coated layers and to consider differences in thickness. These results are shown in Fig. 7. It can be seen that the permeability of the layers based on the grafted CS are almost perfectly superimposed to the permeability of the layers of pristine CS. Therefore, the chemical modification of CS seems to have no significant effect on barrier properties at least at this degree of grafting. It can be noted that the oxygen permeability of the two nanocomposite layers decreases after the addition of 25 % VMT, this layer possesses a permeability of 6.18.10^{-24} m^3.m/m^2.s.Pa with a thickness of 3.01 μm. Although a higher effect on gas barrier properties could be expected with the addition of 60 % VMT, the detection limit of

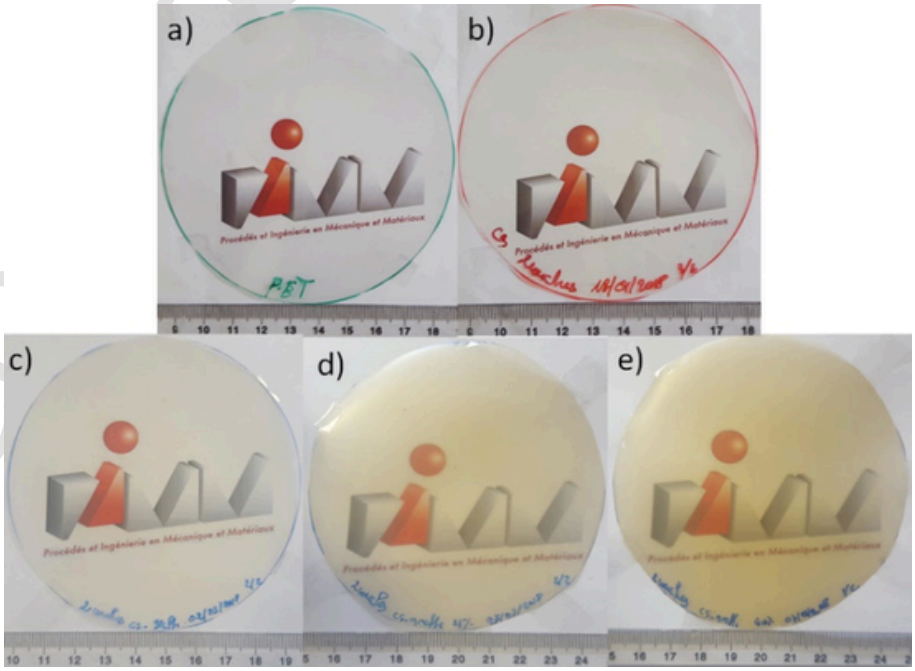

Fig. 5. Images of PET films: a) Uncoated PET b) PET coated with two layers of CS c) PET coated with two layers of CS-g-PA d) PET coated with two layers of CS-g-PA and 25 wt% VMT e) PET coated with two layers of CS-g-PA and 60 wt% VMT.

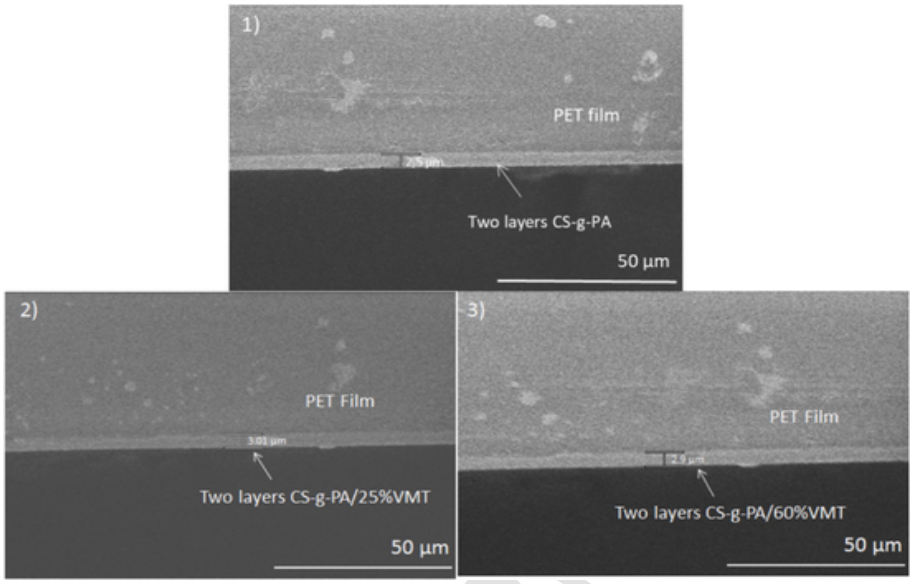

Fig. 6. SEM cross-section micrographs of PET films with different coatings: (1) two layers of CS-g-PA; (2) two layers of CS-g-PA with 25 wt% VMT; (3) two layers of CS-g-PA with 60 wt% VMT.

Table 4
Average thickness of two layers CS-VMT and CS-g-PA/VMT coated PET film measured by SEM.

VMT wt%	Layer thickness (µm)	
	CS/VMT	CS-g-PA/VMT
0	2.1 ± 0.15	2.5 ± 0.1
25	2.6 ± 0.04	3 ± 0.09
60	2.22 ± 0.06	2.8 ± 0.07

the device is reached, preventing the observation of further changes, as shown in Fig. 7 (b). We can conclude that the loss of barrier properties due to grafting does not significantly impact the general behavior under dry conditions.

3.3. Effect of relative humidity on barrier properties of PET film coated CS-g-PA/VMT

After verifying that the barrier properties of grafted CS remain acceptable under dry conditions, it is important to look at the evolution of behavior under humid conditions and compare it to that of pristine CS. Fig. 8 gathers the results of the helium transmission rate measurements of PET films coated with two layers of CS-g-PA and CS-g-PA/VMT at different RH compared to CS and CS/VMT.

At 0 % RH, a decrease in helium permeance is observed between pristine CS and those with grafted CS, regardless of the amount of VMT. This result is quite surprising in comparison to what was observed in OTR where the barrier properties are similar for both cases in Fig. 7 (a). It could mean that the grafting of a hydrophobic chain onto the CS chains decreases the flow of helium compared to oxygen due to their nature. The impact of layer thickness may be a factor explaining this difference since grafted CS shows a greater thickness compared to pristine CS. The behavior at 54 % RH follows the same trend between grafted and non-grafted with stable properties compared to dry conditions, as already observed. From 74 % HR, the tendency of the grafted

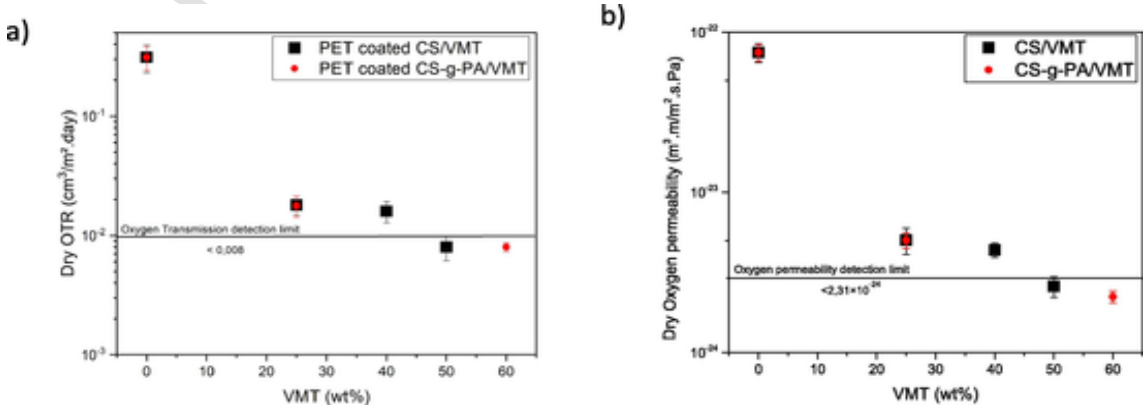

Fig. 7. Oxygen transmission rates of a PET film coated with two layers of CS/VMT and CS-g-PA/VMT with different VMT contents (a) and oxygen permeabilities of those layers (b) in dry conditions (23 °C and 0 % RH).

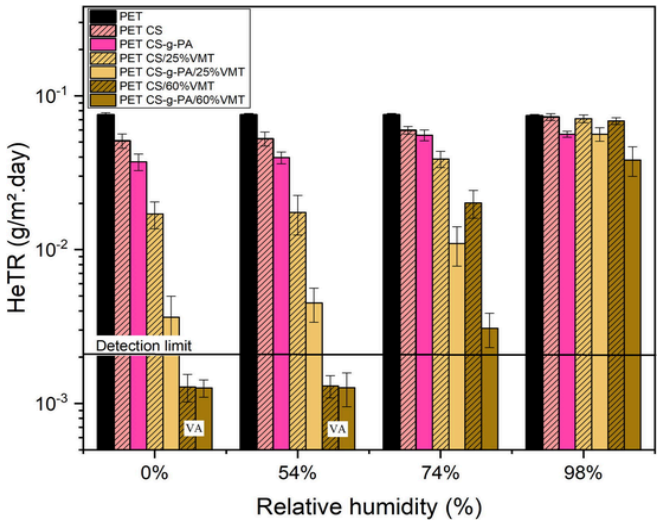

Fig. 8. Helium transmission rate of PET films coated with two layers of CS/VMT and CS-g-PA/VMT at different humidity rates with 25 wt% and 60 wt% VMT (VA: approximate values since the detection limit has been exceeded).

CS is the same as that of the non-grafted, namely, an increase in the permeance of the film. However, in the films produced, there are still lower permeance values with CS-g-PA coating. Finally, at 98 % RH, the permeability is strongly increased for all cases. However, the CS-g-PA coated PET containing 60 wt% VMT still has a lower value than simple PET. An improvement of a factor 2 is observed in these extreme conditions (0.073 g/m^2.day for PET and 0.038 g/m^2.day for PET coated with CS-g-PA/60 wt% VMT). In order to eliminate the fact that the layers do not all have the same thickness, the permeability of the coated layers was calculated using measured thicknesses and permeance values. It is noted that the permeability of the grafted CS layers (Fig. 9) remains better than the one of pristine CS, regardless of conditions. However, the difference in permeability is much clearer with the incorporation of VMT into the coating. The combined effect of grafting and addition of vermiculite would appear to limit the impact of moisture on the barrier properties of the material up to 74 % RH only. The improvement due to grafting is particularly noticeable under the most humid conditions. This is expected, as the hydrophilicity is slightly modified by the addition of the grafts, making their effect more visible at higher relative humidity. As a result, films prepared with CS-g-PA show better results compared to CS-based films in wet conditions, as anticipated. Thus, this suggests a synergistic effect of grafting and VMT on the helium barrier properties of CS.

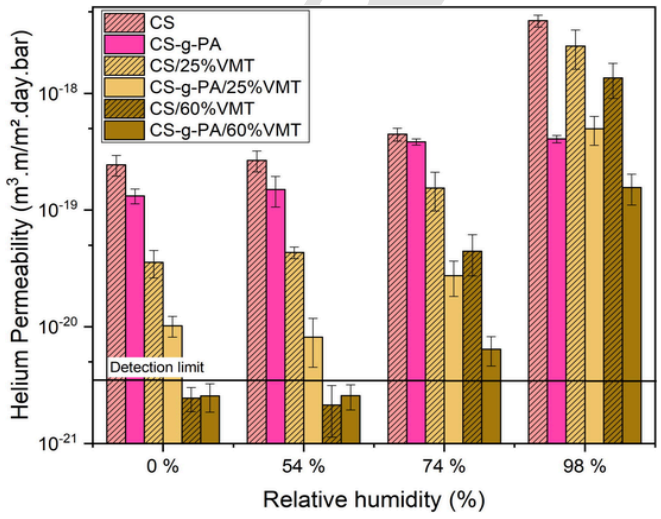

Fig. 9. Helium permeability of two coated layers of CS, CS-g-PA, CS/VMT and CS-g-PA/VMT at different humidity rates with 25 wt% and 60 wt% VMT (VA: approximate values since the detection limit was exceeded).

4. Conclusion

In this study, we have shown that the permeability of coated CS and CS/VMT layers remains stable up to 54 % relative humidity and that, from 74 % relative humidity, the layers gradually lose their barrier properties regardless of the nanofillers content. At 98 % RH, all barrier properties of coatings are almost completely lost and the permeance of the film corresponds closely to that of PET alone. To improve this critical point from an application point of view, the grafting of a fatty acid, palmitic acid, on the CS chain was successfully carried out.^{13}C NMR solid phase analysis confirmed the presence of peaks corresponding to the methyl groups of palmitic acid (CH_2) in the CS-g-PA NMR spectrum after the elimination step of unreacted palmitic acid. DSC thermogram of CS-g-PA shows no peak corresponding to the melting of the palmitic acid, which is therefore prohibited from crystallizing suggesting the grafting of the PA molecules onto the CS backbone.

In addition, the solubility test has proven that CS-g-PA is not soluble in an acidified aqueous solution, which is a good solvent of pristine CS implying also the efficiency of the grafting reaction. Then to analyze the impact of the presence of a lateral alkylated chain onto the CS, the evolution of helium barrier properties of the CS and CS/VMT film at all RH conditions was carried out and confirmed that the increase of hydrophobicity, at this rate of grafting, improves the barrier properties in the different humid conditions without any loss of those excellent properties in the dry state.

Indeed, at 74 % RH, an improvement factor close to 30 is obtained compared to pure PET with a CS-g-PA coating and 60 wt% VMT. At the same humidity content, the helium permeability value of this sample (CS-g-PA/60 wt%VMT) is measured at 6.4x10^{-21} m^3/m^2.Pa with a layer thickness of 2.9 μm. These improvements suggest that this type of grafting of long alkylated chains might be interesting to prevent the effect of humidity on barrier properties for hydrophilic polymers.

CRediT authorship contribution statement

Fatima Essabti: Writing – original draft, Investigation, Funding acquisition, Formal analysis. **Alain Guinault:** Writing – review & editing, Methodology, Investigation, Formal analysis. **Sébastien Roland:** Writing – review & editing, Methodology, Investigation. **Matthieu Gervais:** Writing – review & editing, Visualization, Supervision, Investigation, Conceptualization.

Declaration of competing interest

The authors declare the following financial interests/personal relationships which may be considered as potential competing interests: [Fatima Essabti reports financial support was provided by Islamic Development Bank of the kingdom of Saudi Arabia. If there are other authors, they declare that they have no known competing financial interests or personal relationships that could have appeared to influence the work reported in this paper.].

Acknowledgements

The work was supported by the Islamic Development Bank of the kingdom of Saudi Arabia with the PhD funding.

We thank Cédric Lorthioir from Pierre and Marie Curie University (UPMC) for NMR measurements, Thomas Karbowiak and Frédéric Debeaufort at the University of Bourgogne for comments that greatly improved the manuscript.

Data availability

Data will be made available on request.

References

[1] F. Wu, M. Misra, A.K. Mohanty, Challenges and new opportunities on barrier performance of biodegradable polymers for sustainable packaging, Prog. Polym. Sci. 117 (2021) 101395, https://doi.org/10.1016/j.progpolymsci.2021.101395.

[2] S. Kumar, A. Mukherjee, J. Dutta, Chitosan based nanocomposite films and coatings: emerging antimicrobial food packaging alternatives, Trends Food Sci. Technol. 97 (2020) 196–209, https://doi.org/10.1016/j.tifs.2020.01.002.

[3] B. Qu, Y. Luo, A review on the preparation and characterization of chitosan-clay nanocomposite films and coatings for food packaging applications, Carbohydr. Polym. Technol. Appl. 2 (2021) 100102, https://doi.org/10.1016/j.carpta.2021.100102.

[4] Y. Zhao, Y. Zhang, H. Dong, W. Wu, X. Yang, Q. He, Functional biopolymers for food packaging: formation mechanism and performance improvement of chitosan based composites, Food Biosci. 54 (2023) 102927, https://doi.org/10.1016/j.fbio.2023.102927.

[5] F. Croisier, C. Jérôme, Chitosan-based biomaterials for tissue engineering, Eur. Polym. J. 49 (2013) 780–792, https://doi.org/10.1016/j.eurpolymj.2012.12.009.

[6] Y. Wang, E. Wang, Z. Wu, H. Li, Z. Zhu, X. Zhu, Y. Dong, Synthesis of chitosan molecularly imprinted polymers for solid-phase extraction of methyltestenolone, Carbohydr Polym 101 (2014) 517–523, https://doi.org/10.1016/j.carbpol.2013.09.078.

[7] J. Wang, C. Chen, Chitosan-based biosorbents: modification and application for biosorption of heavy metals and radionuclides, Bioresour. Technol. 160 (2014) 129–141, https://doi.org/10.1016/j.biortech.2013.12.110.

[8] M.O. Abd El-Magied, A.A. Galhoum, A.A. Atia, A.A. Tolba, M.S. Maize, T. Vincent, E. Guibal, Cellulose and chitosan derivatives for enhanced sorption of erbium(III), in: Colloids and Surfaces a: Physicochemical and Engineering Aspects 529, 2017, pp. 580–593, https://doi.org/10.1016/j.colsurfa.2017.05.031.

[9] S.K. Shukla, A.K. Mishra, O.A. Arotiba, B.B. Mamba, Chitosan-based nanomaterials: A state-of-the-art review, Int. J. Biol. Macromol. 59 (2013) 46–58, https://doi.org/10.1016/j.ijbiomac.2013.04.043.

[10] R. Jayakumar, M. Prabaharan, R.L. Reis, J.F. Mano, Graft copolymerized chitosan—present status and applications, Carbohydr. Polym. 62 (2005) 142–158, https://doi.org/10.1016/j.carbpol.2005.07.017.

[11] S. Lazar, O. Garcia-Valdez, E. Kennedy, P. Champagne, M. Cunningham, J. Grunlan, Crosslinkable-chitosan-enabled moisture-resistant multilayer gas barrier thin film, Macromol. Rapid Commun. 40 (2019) 1800853, https://doi.org/10.1002/marc.201800853.

[12] M. Božič, S. Gorgieva, V. Kokol, Laccase-mediated functionalization of chitosan by caffeic and gallic acids for modulating antioxidant and antimicrobial properties, Carbohydr. Polym. 87 (2012) 2388–2398, https://doi.org/10.1016/j.carbpol.2011.11.006.

[13] Y.-S. Cho, S.-K. Kim, C.-B. Ahn, J.-Y. Je, Preparation, characterization, and antioxidant properties of gallic acid-grafted-chitosans, Carbohydr. Polym. 83 (2011) 1617–1622, https://doi.org/10.1016/j.carbpol.2010.10.019.

[14] S.-H. Yu, F.-L. Mi, J.-C. Pang, S.-C. Jiang, T.-H. Kuo, S.-J. Wu, S.-S. Shyu, Preparation and characterization of radical and pH-responsive chitosan–gallic acid conjugate drug carriers, Carbohydr. Polym. 84 (2011) 794–802, https://doi.org/10.1016/j.carbpol.2010.04.035.

[15] W. Pasanphan, S. Chirachanchai, Conjugation of gallic acid onto chitosan: An approach for green and water-based antioxidant, Carbohydr. Polym. 72 (2008) 169–177, https://doi.org/10.1016/j.carbpol.2007.08.002.

[16] J. Liu, J. Lu, J. Kan, Y. Tang, C. Jin, Preparation, characterization and antioxidant activity of phenolic acids grafted carboxymethyl chitosan, Int. J. Biol. Macromol. 62 (2013) 85–93, https://doi.org/10.1016/j.ijbiomac.2013.08.040.

[17] J. Liu, J. Lu, J. Kan, C. Jin, Synthesis of chitosan-gallic acid conjugate: structure characterization and in vitro anti-diabetic potential, Int. J. Biol. Macromol. 62 (2013) 321–329, https://doi.org/10.1016/j.ijbiomac.2013.09.032.

[18] A.O. Aytekin, S. Morimura, K. Kida, Synthesis of chitosan–caffeic acid derivatives and evaluation of their antioxidant activities, J. Biosci. Bioeng. 111 (2011) 212–216, https://doi.org/10.1016/j.jbiosc.2010.09.018.

[19] Y. Liu, B. Zhang, V. Javvaji, E. Kim, M.E. Lee, S.R. Raghavan, Q. Wang, G.F. Payne, Tyrosinase-mediated grafting and crosslinking of natural phenols confer functional properties to chitosan, Biochem. Eng. J. 89 (2014) 21–27, https://doi.org/10.1016/j.bej.2013.11.016.

[20] J.C. Shiu, M.-H. Ho, S.-H. Yu, A.-C. Chao, Y.-R. Su, W.-J. Chen, Z.-C. Chiang, W.P. Yang, Preparation and characterization of caffeic acid grafted chitosan/CPTMS hybrid scaffolds, Carbohydr. Polym. 79 (2010) 724–730, https://doi.org/10.1016/j.carbpol.2009.09.025.

[21] A. Aljawish, L. Muniglia, J. Jasniewski, A. Klouj, J. Scher, I. Chevalot, Adhesion and growth of HUVEC endothelial cells on films of enzymatically functionalized chitosan with phenolic compounds, Process Biochem. 49 (2014) 863–871, https://doi.org/10.1016/j.procbio.2014.02.001.

[22] S. Woranuch, R. Yoksan, Preparation, characterization and antioxidant property of water-soluble ferulic acid grafted chitosan, Carbohydr. Polym. 96 (2013) 495–502, https://doi.org/10.1016/j.carbpol.2013.04.006.

[23] E. Aracri, A. Fillat, J.F. Colom, A. Gutiérrez, J.C. del Río, Á.T. Martínez, T. Vidal, Enzymatic grafting of simple phenols on flax and sisal pulp fibres using laccases, Bioresour. Technol. 101 (2010) 8211–8216, https://doi.org/10.1016/j.biortech.2010.05.080.

[24] E. Aracri, M.B. Roncero, T. Vidal, Studying the effects of laccase-catalysed grafting of ferulic acid on sisal pulp fibers, Bioresour. Technol. 102 (2011) 7555–7560, https://doi.org/10.1016/j.biortech.2011.05.046.

[25] G.-B. Jiang, Z.-T. Lin, X.-J. Xu, Hai Zhang, K. Song, Stable nanomicelles based on chitosan derivative: in vitro antiplatelet aggregation and adhesion properties, Carbohydr. Polym. 88 (2012) 232–238, https://doi.org/10.1016/j.carbpol.2011.11.089.

[26] W. Zhu, Z. Zhang, Preparation and characterization of catechin-grafted chitosan with antioxidant and antidiabetic potential, Int J Biol Macromol 70 (2014) 150–155, https://doi.org/10.1016/j.ijbiomac.2014.06.047.

[27] I. Brzonova, W. Steiner, A. Zankel, G.S. Nyanhongo, G.M. Guebitz, Enzymatic synthesis of catechol and hydroxyl-carboxic acid functionalized chitosan microspheres for iron overload therapy, Eur. J. Pharm. Biopharm. 79 (2011) 294–303, https://doi.org/10.1016/j.ejpb.2011.04.018.

[28] F. Chen, Z. Shi, K.g. Neoh, E. t. Kang, Antioxidant and antibacterial activities of eugenol and carvacrol-grafted chitosan nanoparticles, Biotechnology and Bioengineering 104 (2009) 30–39, https://doi.org/10.1002/bit.22363.

[29] O. Sauperl, J. Tompa, J. Volmajer-Valh, Influence of the temperature on the efficiency of cellulose treatment using copolymer chitosan-eugenol, J. Eng. Fibers Fabr. 9 (2014) 155892501400900320, https://doi.org/10.1177/155892501400900312.

[30] J.-Y. Woo, J.-Y. Je, Antioxidant and tyrosinase inhibitory activities of a novel chitosan–phloroglucinol conjugate, Int. J. Food Sci. Technol. 48 (2013) 1172–1178, https://doi.org/10.1111/ijfs.12071.

[31] X. Liu, X. Sun, H. Du, Y. Li, Y. Wen, Z. Zhu, A transparent p-coumaric acid-grafted-chitosan coating with antimicrobial, antioxidant and antifogging properties for fruit packaging applications, Carbohydr. Polym. (2024) 122238, https://doi.org/10.1016/j.carbpol.2024.122238.

[32] M. Božič, S. Gorgieva, V. Kokol, Homogeneous and heterogeneous methods for laccase-mediated functionalization of chitosan by tannic acid and quercetin, Carbohydr. Polym. 89 (2012) 854–864, https://doi.org/10.1016/j.carbpol.2012.04.021.

[33] M. Curcio, F. Puoci, F. Iemma, O.I. Parisi, G. Cirillo, U.G. Spizzirri, N. Picci, Covalent insertion of antioxidant molecules on chitosan by a free radical grafting procedure, J. Agric. Food Chem. 57 (2009) 5933–5938, https://doi.org/10.1021/jf900778u.

[34] S.K. Swain, S.K. Kisku, G. Sahoo, Preparation of thermal resistant gas barrier chitosan nanobiocomposites, Polym. Compos. 35 (2014) 2324–2328, https://doi.org/10.1002/pc.22897.

[35] F. Essabti, A. Guinault, S. Roland, G. Régnier, S. Ettaqi, M. Gervais, Preparation and characterization of poly(ethylene terephthalate) films coated by chitosan and vermiculite nanoclay, Carbohydr. Polym. 201 (2018) 392–401, https://doi.org/10.1016/j.carbpol.2018.08.077.